Mon. Not. R. Astron. Soc. **358,** 781–794 (2005) doi:10.1111/j.1365-2966.2005.08722.x

Short time-scale optical variability of the dwarf Seyfert nucleus in NGC 4395

J. E. Skelton,[1⋆] A. Lawrence,[1] A. Pappa,[1] P. Lira[2] and O. Almaini[1,3]

[1]*Institute for Astronomy, University of Edinburgh, Royal Observatory, Blackford Hill, Edinburgh EH9 3HJ*
[2]*Departamento de Astronomíca, Universidad de Chile, Casilla 36-D, Santiago, Chile*
[3]*School of Physics and Astronomy, University of Nottingham, University Park, Nottingham NG7 2RD*

Accepted 2004 December 7. Received 2004 December 2; in original form 2004 October 14

ABSTRACT

We present optical spectroscopic observations of the least-luminous known Seyfert 1 galaxy, NGC 4395, which was monitored every half-hour over the course of three nights. The continuum emission varied by ∼35 per cent over the course of three nights and we find marginal evidence for greater variability in the blue continuum than the red. A number of diagnostic checks were performed on the data in order to constrain any systematic or aperture effects. No correlations were found that adequately explained the observed variability, hence we conclude that we have observed real intrinsic variability of the nuclear source. No simultaneous variability was measured in the broad Hβ line, although given the difficulty in deblending the broad and narrow components it is difficult to comment on the significance of this result. The observed short time-scale continuum variability is consistent with NGC 4395 having an intermediate-mass ($\sim 10^5\,M_\odot$) central supermassive black hole, rather than a very low accretion rate. Comparison with the Seyfert 1 galaxy NGC 5548 shows that the observed variability seems to scale with black hole mass in roughly the manner expected in accretion models. However, the absolute time-scale of variability differs by several orders of magnitude from that expected in simple accretion disc models in both cases.

Key words: galaxies: active – galaxies: individual: NGC 4395 – galaxies: Seyfert.

1 INTRODUCTION

NGC 4395 is a nearby, late-type spiral galaxy of morphological type Sd III–IV. It exhibits a very low surface-brightness disc, with almost no central bulge and loose spiral arms showing some isolated regions of star formation. Optical spectra of the faint, star-like nucleus reveal strong, narrow forbidden emission lines from a wide range of species and ionization, as well as weak broad wings on permitted lines. Filippenko & Sargent (1989) interpreted these observations as an indication that NGC 4395 harboured an extremely low-luminosity Seyfert 1 nucleus. Subsequent multiwavelength observations (Sramek 1992; Filippenko, Ho & Sargent 1993) confirmed this classification and convincingly argued against other origins for the observed non-stellar emission. With an absolute blue magnitude of ∼−11, the nucleus of NGC 4395 has a lower luminosity than the brightest supergiant stars and is a factor of $\sim 10^4$ fainter than even low-luminosity classical Seyfert 1 galaxies such as NGC 4051, making it the least-luminous Seyfert 1 discovered to date.

There are two likely possibilities for the very low luminosity nucleus in NGC 4395. One is a low accretion rate, in line with other low-luminosity active galactic nuclei (AGN; Ptak et al. 1998). The other is that the central supermassive black hole is significantly smaller than in more luminous AGN, with a relative accretion rate that is more typical of classical Seyferts giving rise to the observed properties of NGC 4395. Given that NGC 4395 is a small late-type spiral with a very low luminosity bulge component, a small central black hole is consistent with the observed correlation between bulge mass and black hole mass (Ferrarese & Merritt 2000; Gebhardt et al. 2000). Several estimates of the black hole mass in NGC 4395 have been made. A firm upper limit of $6.2 \times 10^6\,M_\odot$ has been placed by Filippenko & Ho (2003) using velocity dispersion analysis of the Ca II near-infrared(IR) triplet. However, this is a measure of the virial mass of the entire nuclear stellar cluster and the mass of the actual black hole could be considerably smaller. Estimates using photoionization modelling of the broad-line region (Kraemer et al. 1999) and from power-law fitting to the fluctuation power density spectrum (PDS; Shih, Iwasawa & Fabian 2003) give consistent estimates in the region 10^4–$10^5\,M_\odot$. These values are lower by several orders of magnitude than those found in other typical Seyfert galaxies and, while neither of these methods is particularly accurate, it is encouraging that the estimates are consistent with one another.

One test of the size of the central engine in NGC 4395 is fast multiwavelength variability. Smaller scalelengths imply that the

⋆E-mail: jes@roe.ac.uk

light- and sound-crossing time-scales should be shorter, leading to variability on short time-scales. An early optical monitoring campaign over several years by Shields & Filippenko (1992) reported that NGC 4395 showed no variability in either the broad lines or the continuum. However, a subsequent spectroscopic study by Lira et al. (1999) found continuum variability over a time-scale of 6 month of factors of order 2 and 1.3 in the blue and red, respectively. Variability in the broad lines was also found, although with a smaller amplitude than that seen in the continuum. Lira et al. also analysed broad-band photometric images (*B* and *I* bands) and detected variability of order 20 per cent between nights. Optical spectroscopic data on NGC 4395 have also been obtained over a number of years at Lick Observatory (Kraemer et al. 1999). When these data were investigated to determine whether they showed variability similar to that seen by Lira et al., they found no evidence of the factor of 2 variations but more modest variability could not be ruled out (Moran et al. 1999).

A well-studied correlation is seen to exist between the amplitude of the variability in X-rays and the intrinsic luminosity of the nucleus for local AGN (Nandra et al. 1997; Turner et al. 1999; Almaini et al. 2000; Manners, Almaini & Lawrence 2002), showing that higher luminosity AGN exhibit lower amplitude variability. In contrast, many low-luminosity AGN (typical X-ray luminosity 0.4–60×10^{40} erg s^{-1}) in nearby large galaxies show very little variability in X-rays, which has been interpreted as evidence for an inefficient accretion process such as an advection-dominated accretion flow (Ptak et al. 1998). NGC 4395 has been well studied at X-ray wavelengths and fast, large amplitude variability has been observed in this object. Lira et al. (1999) found variability of approximately a factor of 2 over a time-scale of 15 d from *ROSAT* Position Sensitive Proportional Counter (PSPC; 0.1–2.4 keV) data. Such variability is not particularly fast for Seyfert 1 AGN. However, subsequent variability studies with better sensitivity and time resolution in the harder 2–10 keV band using *ASCA* found X-ray flux changes on time-scales of approximately 100 s to 12 h, with the shortest doubling time-scale found to be of order 100 s (Iwasawa et al. 2000). Follow-up *ASCA* observations (Shih et al. 2003) confirmed the earlier findings and estimated the PDS in the 1.2–10 and 2–10 keV bands, with the possible detection of a break in the best-fitting power law. These findings suggest that, while other dwarf Seyferts may have normal-size central engines but radiatively inefficient accretion processes, NGC 4395 is accreting at a normal fraction of the Eddington limit but genuinely contains a small central engine when compared with other classical Seyfert 1 galaxies.

To test the hypothesis that the Seyfert nucleus in NGC 4395 contains a small central black hole, we have undertaken optical spectroscopic observations of NGC 4395 with the aim of monitoring the nuclear region every ∼30 min for several consecutive nights. The motives for this study were several: first, it was important to check whether the short time-scale variability observed in the broad-band optical observations of Lira et al. (1999) was characteristic of NGC 4395 or a freak event and, secondly, we wished to determine whether the variability seen in NGC 4395 had different characteristics to classical Seyfert 1 galaxies, in both amplitude and time-scale. Although the absolute flux calibration of spectroscopic observations is often less accurate than for broad-band photometry, a careful observing procedure can reduce the uncertainties and allow quantitative statements to be made. The spectroscopic observations had two advantages: if rapid continuum variability was observed, it could be determined (i) whether there was a corresponding colour change and (ii) whether any simultaneous variability was seen in the broad lines. If broad line variability was seen, it was hoped that the time sampling of the observations would allow any lag between the continuum and line variations to be estimated, thus determining whether the size of the broad-line region scales with luminosity (Peterson et al. 2000). In this paper, the detection of optical continuum variability on time-scales of ∼8 h is reported. In Sections 2 and 3, the observations and reduction of the optical spectra are presented. Section 4 describes the analysis procedure and checks that were carried out to determine whether the observed variability was the result of systematic or atmospheric effects, and discusses the observed variability of NGC 4395. The results are discussed with respect to other well-studied AGN and the implications for models of nuclear regions in active galaxies in Section 5. The subsequent conclusions are summarized in Section 6.

2 OBSERVATIONS

Spectra of the nuclear region of NGC 4395 were obtained on 1998 March 17–20 using the 2.5-m Isaac Newton Telescope at the Roque de los Muchachos Observatory. A Tek 1024 × 1024 CCD was used together with an R300V grating. The CCD was windowed to give a scale of 0.7 arcsec pixel^{-1} in the spatial direction and the central wavelength of the observations was 5135 Å, giving a dispersion of 3.32 Å̃pixel^{-1} over a wavelength range of ∼3500–6900 Å.

In order to detect spectral variations of the order of 20 per cent, a meticulous observing strategy was required, because the standard procedure rarely results in better than 30 per cent accuracy in the absolute flux calibration. Our aim in this study was for an accuracy of ∼5 per cent and to realize this the following procedure was implemented.

NGC 4395 was visible at an elevation of $>30^{\circ}$ for the entirety of the four nights. Conditions were cloudless for three of the four nights: the data from night 4 was affected by the presence of high cirrus for part of the night and was scrapped. Slit width was alternated between 2 and 8 arcsec, giving separate interleaved sets of observations of NGC 4395, with a sampling interval of approximately 30 min in both cases. In all observations, the slit was positioned at the parallactic angle to prevent light losses as a result of differential refraction through the atmosphere. The use of two slit widths allowed a number of systematic effects to be corrected for or eliminated entirely. The 2-arcsec slit was used to reduce the contribution of the host galaxy starlight in each spectrum, while the 8-arcsec slit was used to minimize aperture effects as a result of variable seeing conditions, poor centring of the object in the slit and the possibility that the narrow-line region was resolved. This last point is unlikely: analysis of *Hubble Space Telescope* (*HST*) images by both Filippenko et al. (1993) and Lira et al. (1999) found that the nucleus of NGC 4395 had an intrinsic FWHM of less than 0.05 arcsec. Seeing conditions were never better than 1 arcsec during these observations and so we can be confident that resolution of the narrow-line region (NLR) is not a serious consideration in this case. Each NGC 4395 observation was bracketed by observations of photometric standard stars (each observed using both slits at all times). These allowed any variations in both the seeing conditions and atmospheric extinction to be quantified and if necessary corrected for. Bias frames, tungsten flats and twilight sky flats were taken at the beginning and end of each night. A log of the NGC 4395 observations is given in Table 1.

3 DATA REDUCTION

The data were reduced using IRAF software routines and bias correction was performed in the standard way. Pixel-to-pixel sensitivity

Table 1. Journal of NGC 4395 observations.

JD +2450800	Slit width	Exp. time (s)	PA	Airmass	JD +2450800	Slit width	Exp. time (s)	PA	Airmass
		Night 1					Night 2, continued		
90.3959	2	500	104.5	1.791	91.6016	2	1000	121.5	1.012
90.4022	2	500	103.6	1.711	91.6116	8	200	111.1	1.021
90.4090	8	100	102.6	1.633	91.6256	2	1000	103.4	1.039
90.4233	2	1000	100.4	1.496	91.6337	8	200	100.0	1.051
90.4312	8	200	99.2	1.431	91.6474	2	1000	95.8	1.079
90.4453	2	1000	97.0	1.335	91.6552	8	200	93.7	1.098
90.4544	8	200	95.6	1.283	91.6684	2	1000	90.8	1.137
90.4681	2	1000	93.2	1.216	91.6762	8	200	89.2	1.163
90.4761	8	200	91.8	1.183	91.6891	2	1000	86.8	1.215
90.4896	2	1000	89.2	1.135	91.6969	8	200	85.5	1.250
90.4995	8	200	87.0	1.106	91.7025	2	1000	83.4	1.319
90.5125	2	1000	83.6	1.074	91.7175	8	200	82.2	1.368
90.5204	8	200	81.3	1.058	91.7293	2	1000	80.4	1.454
90.5336	2	1000	75.9	1.036	91.7370	8	200	79.2	1.519
90.5429	8	200	71.0	1.024	91.7503	2	1000	77.2	1.652
90.5562	2	1000	58.3	1.012	91.7581	8	200	77.2	1.744
90.5642	8	200	47.3	1.007	91.7676	2	1000	74.6	1.875
90.5763	2	1000	12.8	1.004	91.7725	8	200	73.9	1.952
90.5842	8	200	165.1	1.004					
90.5972	2	1000	132.5	1.008			Night 3		
90.6053	8	200	119.3	1.013					
90.6765	2	500	89.7	1.154	92.4082	2	1000	101.9	1.586
90.6828	2	500	88.5	1.177	92.4262	8	200	99.1	1.428
90.6880	8	200	87.5	1.198	92.4438	2	1000	96.4	1.312
90.7000	2	1000	85.4	1.253	92.4516	8	200	95.1	1.269
90.7080	8	200	84.1	1.294	92.4644	2	1000	92.9	1.209
90.7200	2	1000	82.2	1.368	92.4724	8	200	91.5	1.176
90.7279	8	200	81.0	1.422	92.4856	2	1000	88.8	1.131
90.7398	2	1000	79.2	1.520	92.4934	8	200	87.2	1.107
90.7475	8	200	78.0	1.592	92.5086	2	1000	83.2	1.071
90.7565	2	500	76.7	1.691	92.5164	8	200	80.8	1.055
90.7628	2	500	75.8	1.769	92.5301	2	1000	74.9	1.033
90.7677	8	150	75.0	1.835	92.5381	8	200	70.6	1.023
90.7701	2	100	74.7	1.870	92.5513	2	1000	57.6	1.012
					92.5592	8	200	46.4	1.007
		Night 2			92.5735	2	1000	4.2	1.004
					92.5813	8	200	156.5	1.004
91.3987	2	1000	103.7	1.721	92.5939	2	1000	128.8	1.009
91.4065	8	200	102.5	1.630	92.6016	8	200	117.5	1.014
91.4235	2	1000	100.0	1.471	92.6145	2	1000	107.9	1.027
91.4313	8	200	98.8	1.410	92.6222	8	200	103.5	1.037
91.4455	2	1000	96.6	1.318	92.6363	2	1000	98.3	1.061
91.4534	8	200	95.3	1.274	92.6441	8	200	95.9	1.078
91.4667	2	1000	93.0	1.211	92.6573	2	1000	92.6	1.111
91.4746	8	200	91.6	1.178	92.6650	8	200	90.9	1.134
91.4918	2	1000	88.1	1.120	92.6792	2	1000	88.1	1.185
91.4998	8	200	86.3	1.098	92.6870	8	200	86.7	1.217
91.5203	2	1000	80.3	1.053	92.7002	2	1000	84.5	1.282
91.5284	8	200	77.2	1.039	92.7079	8	200	83.2	1.325
91.5421	2	1000	69.3	1.022	92.7245	2	1000	80.7	1.439
91.5499	8	200	63.3	1.015	92.7324	8	200	79.5	1.502
91.5623	2	1000	43.8	1.007	92.7452	2	1000	77.6	1.626
91.5701	8	200	25.9	1.004	92.7531	8	200	76.4	1.716
91.5822	2	1000	164.4	1.004	92.7661	2	1000	74.4	1.895
91.5900	8	200	140.0	1.006	92.7723	8	200	73.5	1.994

variations were removed using tungsten lamp spectra, which were observed to contain vignetting effects. It was decided to correct these effects using spectra of the twilight sky, as the optical light path for these frames was the same as for the spectra of NGC 4395 itself. Therefore, the tungsten spectrum was first smoothed using a median filter designed to smooth the gain variations but preserve the vignetting features. The unsmoothed flat was then divided through by the smoothed version to produce a flat field that contained information about the pixel-to-pixel variations but no information about the vignetting. Each twilight sky and NGC 4395 spectrum was divided

through by this frame. The vignetting effects were then removed from the NGC 4395 spectrum by dividing through by the processed twilight sky frame that contained the vignetting information.

For wavelength calibration, a low-order polynomial function was fitted to strong lines in a copper–argon comparison spectrum. The precision of the fit was improved by including intermediate lines once a rough determination of the dispersion solution had been found. Dispersion solutions were found every 35 arcsec (50 pixel) along the slit and sixth-order Chebyshev polynomials were fitted to these solutions to correct any geometrical distortions. To remove the sky background, a low-order cubic spline function was fitted along the spatial axis of each spectrum and then subtracted. One-dimensional spectra were extracted using an ∼5-arcsec aperture designed to minimize any contributions from the host galaxy, including nearby H II regions. Lira et al. (1999) estimated the contamination from host galaxy starlight to be at most 10 per cent from measurements of the equivalent width of the ultraviolet Ca II line.

Flux calibration of the extracted NGC 4395 spectra was initially performed in the standard way. Spectrophotometric standard stars were used to determine the sensitivity of the detector over the entire wavelength range. The standard stars used were Feige 34, G191-B2B and HZ44 from Massey et al. (1988), together with BD75+325 and HZ21 from Oke (1990). The standard extinction curve for the Roque de los Muchachos observatory was used to perform the extinction correction. For each NGC 4395 observation, the sensitivity function was constructed using the standard star observations closest in time and using the same slit width. Because an ∼5 per cent accuracy was desired, in order to ensure that the extinction correction had been applied correctly the standard extinction correction was applied to each standard star observation and then the counts s^{-1} Jy^{-1} was measured at 5500 Å (Johnson *V*). Significant variations were seen in the derived calibration both within a night and on a night-to-night basis. To correct for the night-to-night variations, a grey shift correction was applied to all spectra (including both spectrophotometric standards and NGC 4395 observations) based on measurements made on site by the Carlsberg Meridian Circle (CMC). The grey shifts for the three nights were 0.30, 0.20 and 0.13 mag, respectively. To correct for atmospheric variations within each night, the following procedure was implemented. First, the standard star observations taken with the 8-arcsec slit width were corrected to first order using the data from the CMC and the counts s^{-1} Jy^{-1} for each observation were measured. This was done at several different wavelengths to check that any intranight variations were grey, as shown in Fig. 1. The mean of all measurements (at one wavelength) was found and the magnitude shift required to bring each observation to the mean value calculated. The 8-arcsec slit data was used for this purpose because, as a result of the large slit width, we could be reasonably confident that any variations seen were solely the result of variations in atmospheric transparency and not the result of other effects such as seeing changes. The magnitude shifts required to apply the same second-order correction to the NGC 4395 data (both 2- and 8-arcsec slit widths) were then calculated by interpolating between the 8-arcsec standard star observations and individual extinction curves were constructed for each observation. The flux calibration was then repeated using a global sensitivity function calculated for each night and the separate extinction curves. The procedure we have followed assumes that the transparency trends we see in the standard stars are also followed by NGC 4395. The smoothness of the trends suggests this is correct. Any remaining small time-scale transparency fluctuations could produce errors in our derived light curves of NGC 4395. We estimated this by fitting straight lines to the data for each night in Fig. 1 and then calculating the residual variations. This showed that any such short time-scale transparency variations are less than 5 per cent (2σ).

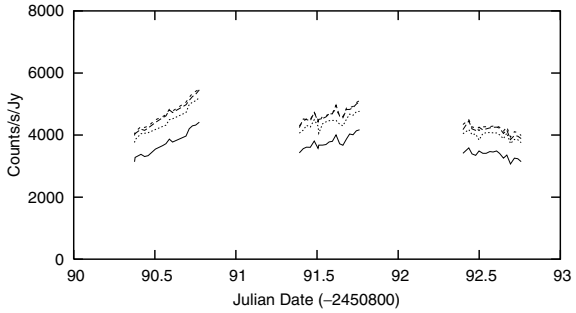

Figure 1. The variation in counts s^{-1} Jy^{-1} over the three photometric nights for the standard stars observed using the 8-arcsec slit. To ensure that any variations were grey, measurements were made at four wavelengths: 4000 Å (solid line), 4500 Å (short dashes), 5500 Å (long dashes) and 6200 Å (dotted).

The combined spectrum is shown in Fig. 2. This has extremely high signal-to-noise ratio and many weak lines can be clearly seen. Most of the structure visible in the lower panel of Fig. 2 is real rather than noise. This spectrum will be discussed in a later paper.

4 ANALYSIS AND RESULTS

4.1 Procedure

We examined the continuum variability of NGC 4395 in two ways. First, using the absolute flux calibration described above, including the second-order transparency corrections; and, secondly, by measuring the equivalent widths (EQW) of narrow lines, which we expect to be particularly reliable. If the size of the narrow-line region is of order ∼10 pc (Filippenko et al. 1993), this gives a light-crossing time in excess of 30 yr and so we would not expect to see any significant variability in the narrow lines on time-scales of hours or days. If this is the case, then measurements of the narrow line equivalent widths give a direct measurement of any continuum variability. A further advantage of this technique is that in the absence of systematic effects the EQW is independent of the absolute flux calibration, and so the principle sources of uncertainty will be the accuracies to which we can measure the relative line and continuum fluxes. Possible sources of systematic errors and aperture effects in the NGC 4395 data have been investigated and are discussed in the next section.

The equivalent widths were obtained by fitting low-order polynomial functions to the continuum region under the emission lines and then fitting a Gaussian profile to the emission lines themselves. The emission lines selected were [O II] 3727 Å, [O III] 5007 Å and [O I] 6300 Å. These lines were selected because they were the strongest unblended lines in the blue, green and red regions of the spectrum. Several wavelength regions were required to allow differences in variability with colour to be quantified. To measure the continuum flux, coordinate ranges close to the relevant emission line were selected that would result in the least contamination of the fit by low signal-to-noise ratio emission lines and a polynomial of order zero or one was fitted to these coordinate ranges. The actual fitting order used was determined by eye. A Gaussian function was then fitted to the emission line to obtain the narrow line flux and hence the equivalent width.

The largest uncertainty in the equivalent widths arises from the continuum flux measurement, particularly for the [O II] 3727-Å line,

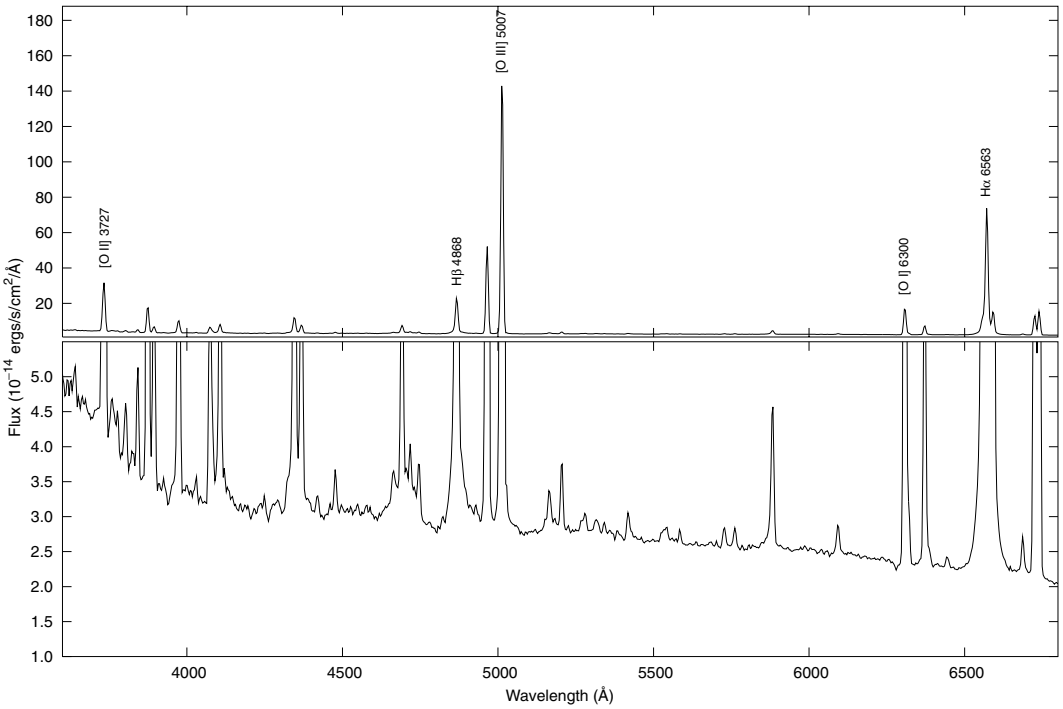

Figure 2. Averaged spectrum for all observations taken using the 2-arcsec slit. The bottom panel has an expanded flux scale showing the low signal-to-noise ratio (S/N) lines.

which has the poorest signal-to-noise ratio in both the 2- and 8-arcsec slit data sets. Two methods were used to quantify this error. First, the continuum fit was manually constrained to lie some distance away from the actual best-fitting value and the effect upon the equivalent width measurement observed. Secondly, the coordinate ranges used for the fitting were changed by small amounts, thus varying the contribution from any low signal-to-noise ratio emission lines, and again the effect upon the equivalent widths determined. The actual uncertainty in the measurement is likely to lie somewhere between these two values, with the fractional error being slightly larger for the [O II] 3727-Å line than either of the other two lines.

Table 2 gives 51 measurements for the equivalent widths, and the continuum and line fluxes for the [O III] 5007-Å and [O I] 6300-Å emission lines, as measured from the 2-arcsec slit data. There are only 50 measurements for the [O II] 3727-Å line, because the signal-to-noise ratio of the last observation on night 1 was too poor in the blue end to allow the measurements to be made. Table 3 contains the measurements made using data from the 8-arcsec slit measurements. There are 48 measurements for both the [O III] 5007-Å and [O I] 6300-Å lines, but similarly only 47 for the [O II] 3727-Å line. The final light curves produced from these data are shown in Figs 3 (2-arcsec slit) and 4 (8-arcsec slit). To allow the measurements from the different emission lines to be compared directly, all light curves have been scaled using the mean equivalent width for each line.

Measurements of the Hβ line flux were also carried out and a similar procedure to that described in Lira et al. (1999) was followed. First, the zero and slope of the continuum region under the Hβ line were determined by eye and then these parameters were fixed during the fitting process. The line itself was fitted using two Gaussians. The narrow component of the line was fitted using a Gaussian of fixed instrumental width determined from the nearby narrow lines, with the amplitude and centre as free parameters. The broad component was fitted using a Gaussian in which the amplitude, width and centre were all free parameters. This procedure was only possible for the 2-arcsec slit data, because the poorer signal-to-noise ratio of the 8-arcsec slit data as a result of starlight contamination from the host galaxy meant that it was difficult to distinguish the weak broad wings on the Hβ line from the continuum. The measured narrow- and broad-component fluxes are given in columns (11) and (12) of Table 2, and an example fit and residuals is shown in Fig. 5. The measured FWHM for the narrow and broad components were $\sim$250 km s^{-1} (fixed using the instrumental resolution) and $\sim$1800 km s^{-1}, respectively. Previous studies give values of $\leqslant$50 km s^{-1} for the narrow component using high-resolution spectroscopy (Filippenko & Sargent 1989) and $\sim$1500 km s^{-1} for the broad component (Kraemer et al. 1999).

4.2 Diagnostic checks

Figs 3 and 4 show short time-scale variations of the nucleus of NGC 4395 throughout all three nights. In order to determine whether these variations were real intrinsic variations of the source, or a result of aperture or systematic effects, a number of diagnostic checks were implemented.

Although NGC 4395 is a very low surface-brightness galaxy, it none the less shows a number of isolated knots of star formation and H II regions. Because the slit was positioned always at the parallactic angle, this resulted in the position angle of the slit relative to the galaxy rotating over the course of observations of the night. Over the course of the observations, therefore, the inclusion and exclusion of any host galaxy features within the slit would have varied. To combat this, a narrow aperture was used during the extraction procedure, rather than performing an optimal extraction using a weighted function over the entire cross-dispersive axis. To check whether any emission from extended regions had been inadvertently included in the extraction aperture in spite of our precautions, a small ($\sim$20 pixel) section of the cross-dispersive axis covering the [O III]

Table 2. Equivalent width, line flux and continuum flux measurements for the 2-arcsec slit data.

JD	[O II] λ3727 Å			[O III] λ5007 Å			[O I] λ6300 Å			Hβ	
+2450800	EQW	Line[1]	Cont[2]	EQW	Line	Cont	EQW	Line	Cont	Narrow	Broad
90.3959311	58.6	4.558	7.775	469	22.80	4.861	57.7	2.325	4.027	1.827	0.935
90.4022447	64.8	4.946	7.637	463	23.95	5.168	58.7	2.487	4.235	2.005	0.910
90.4233443	63.8	5.726	8.974	468	28.42	6.075	59.8	2.914	4.869	2.400	1.002
90.4453813	66.3	5.463	8.243	461	25.60	5.551	61.8	2.538	4.108	2.085	1.071
90.4681417	61.7	5.674	9.195	456	27.15	5.957	57.5	2.823	4.912	2.189	0.949
90.4896174	53.0	5.645	10.65	444	29.69	6.694	57.5	3.156	5.491	2.424	1.058
90.5125167	49.0	5.326	10.86	400	26.81	6.703	57.1	3.111	5.451	2.485	1.054
90.5336336	50.8	4.950	9.738	422	26.82	6.359	57.5	3.007	5.232	2.440	0.980
90.5562956	57.3	5.374	9.374	441	28.37	6.426	59.4	3.189	5.366	2.505	1.066
90.5763477	57.8	5.267	9.105	435	26.73	6.147	58.3	2.979	5.110	2.401	0.980
90.5972456	63.6	4.924	7.748	482	26.67	5.533	61.0	3.116	5.111	2.276	0.965
90.6765387	67.0	6.263	9.353	483	27.74	5.748	63.6	2.864	4.500	2.363	0.951
90.6828755	68.4	5.857	8.559	493	27.23	5.527	62.1	2.745	4.421	2.181	1.103
90.7000862	62.7	5.737	9.152	490	28.36	5.788	64.0	2.932	4.584	2.426	1.008
90.7200977	59.0	5.479	9.280	485	29.07	5.994	63.3	2.927	4.625	2.471	1.110
90.7398720	63.8	5.763	9.030	460	27.22	5.915	59.9	2.828	4.725	2.225	1.093
90.7565387	63.9	5.343	8.362	441	23.49	5.329	58.7	2.462	4.195	1.889	0.991
90.7628350	56.0	5.432	9.693	459	24.89	5.419	59.8	2.606	4.360	1.950	1.032
90.7701035				435	23.33	5.386	55.2	2.416	4.373		
91.3987031	61.0	3.997	6.556	402	19.84	4.937	55.9	2.429	4.343	1.815	0.935
91.4235642	57.9	5.038	8.708	442	25.25	5.716	57.7	2.699	4.674	2.122	1.018
91.4455433	57.8	5.008	8.670	447	24.99	5.592	60.0	2.581	4.304	2.230	1.001
91.4667008	49.8	4.504	9.042	437	25.82	5.906	57.4	2.628	4.593	2.246	1.058
91.4918165	47.4	4.521	9.543	411	24.81	6.042	58.2	2.705	4.646	2.294	1.041
91.5203003	57.6	5.430	9.421	432	26.20	6.066	55.9	2.704	4.840	2.259	1.083
91.5421116	50.4	4.608	9.140	418	24.06	5.758	54.3	2.396	4.415	2.221	1.083
91.5623142	55.8	5.045	9.048	437	24.82	5.679	57.6	2.450	4.256	2.246	1.038
91.5822621	52.9	4.834	9.141	466	27.06	5.810	60.5	2.711	4.481	2.433	0.946
91.6016718	55.1	4.786	8.692	452	25.34	5.603	60.2	2.865	4.757	2.227	1.001
91.6256822	58.2	4.885	8.390	435	24.74	5.692	61.5	2.898	4.715	2.196	1.045
91.6474646	54.4	4.824	8.861	428	23.29	5.443	59.3	2.619	4.417	2.215	1.030
91.6684774	57.1	5.483	9.601	478	29.28	6.121	61.5	3.029	4.923	2.564	1.080
91.6891660	58.8	5.159	8.769	485	26.28	5.417	64.2	2.802	4.362	2.239	1.024
91.7096753	66.8	4.850	7.263	476	23.58	4.957	64.3	2.568	3.995	2.011	0.983
91.7293165	62.3	5.259	8.436	472	27.07	5.736	64.8	3.065	4.733	2.205	1.138
91.7503119	58.5	4.916	8.399	462	24.80	5.368	59.1	2.599	4.399	2.097	0.957
92.4082054	60.1	5.293	8.799	439	26.54	6.049	54.1	2.827	5.223	2.232	1.075
92.4438362	57.2	5.267	9.203	437	26.89	6.152	58.3	2.944	5.049	2.513	1.103
92.4644959	52.1	5.063	9.714	461	28.51	6.181	62.6	2.999	4.792	2.633	1.216
92.4856764	56.2	5.014	8.914	487	27.28	5.598	61.4	2.848	4.636	2.513	1.072
92.5086510	56.3	4.930	8.763	500	27.79	5.563	65.0	2.946	4.531	2.556	1.086
92.5301961	62.7	5.185	8.275	523	28.85	5.514	65.6	2.905	4.431	2.549	1.045
92.5513535	65.0	5.152	7.929	546	29.13	5.334	64.7	2.827	4.372	2.690	1.081
92.5735642	72.8	5.080	6.979	555	26.85	4.752	68.6	2.700	3.934	2.360	1.006
92.5939288	69.1	5.268	7.627	573	29.02	5.065	67.9	2.860	4.214	2.476	1.041
92.6145017	71.8	5.686	7.918	579	29.87	5.157	73.0	3.036	4.161	2.504	1.043
92.6363651	80.9	6.584	8.140	559	31.49	5.635	71.4	3.232	4.524	2.682	1.092
92.6573258	87.1	6.006	6.893	574	27.40	4.843	69.9	2.777	3.974	2.224	0.973
92.6792123	84.9	7.328	8.634	562	32.68	5.814	70.4	3.390	4.817	2.713	1.045
92.7002193	81.0	7.207	8.893	534	32.69	6.120	70.1	3.563	5.085	2.588	1.111
92.7452077	80.1	5.399	6.742	541	26.84	4.960	69.2	2.794	4.038	2.130	0.983

[1]Line fluxes in units of 10^{-14} erg s^{-1} cm^{-2}.
[2]Continuum fluxes in units of 10^{-16} erg s^{-1} cm^{-2} Å^{-1}.

5007-Å line of each two-dimensional spectrum was summed and then checked to see whether there had been any contamination by nearby features such as H II regions. No variable contamination was found.

To double-check this, the equivalent widths, line fluxes and continuum fluxes were plotted versus the slit position angle (PA) to check for correlations (Fig. 6). No correlations are seen with any of these variables and so we are confident that any observed variability does not arise from variable contributions from H II or star-forming regions. The lack of correlations also rules out variability resulting from changing ellipticity of the host galaxy core in the slit.

Table 3. Equivalent widths, continuum and line flux measurements for 8-arcsec slit observations.

JD	[O II] λ3727 Å			[O III] λ5007 Å			[O I] λ6300 Å		
+2450800	EQW	Line[1]	Cont[2]	EQW	Line	Cont	EQW	Line	Cont
90.4090040	77.9	7.020	9.015	411	27.39	6.660	56.4	3.031	5.376
90.4312551	72.0	6.254	8.685	439	27.60	6.291	56.3	3.011	5.351
90.4544959	66.8	6.492	9.719	394	27.29	6.921	54.8	3.212	5.861
90.4761452	56.8	5.800	10.21	411	29.15	7.098	48.6	3.144	6.471
90.4995480	60.4	6.721	11.12	390	29.10	7.454	49.7	3.111	6.263
90.5204855	65.7	6.812	10.37	400	29.74	7.433	50.5	3.200	6.339
90.5429507	73.9	7.468	10.11	389	28.58	7.343	53.2	3.291	6.184
90.5642586	64.1	6.410	10.00	408	28.22	6.924	54.4	3.147	5.782
90.5842470	65.8	6.561	9.976	405	28.04	6.920	51.4	3.025	5.880
90.6053176	67.6	6.286	9.292	425	29.37	6.907	56.8	3.348	5.894
90.6880549	80.4	6.263	7.793	442	27.90	6.316	55.5	3.102	5.590
90.7080896	70.2	6.074	8.650	444	27.59	6.208	56.5	3.126	5.529
90.7279623	72.6	6.462	8.896	426	27.79	6.522	55.0	3.013	5.475
90.7475341	71.9	6.593	9.166	401	28.49	7.107	51.4	3.123	6.076
90.7677135				402	27.71	6.887	51.2	2.987	5.838
91.4065966	64.4	6.564	10.19	390	27.12	6.948	51.4	2.968	5.778
91.4313883	62.0	5.565	8.971	410	25.63	6.246	54.1	2.791	5.159
91.4534484	65.1	6.215	9.551	405	27.55	6.802	53.7	2.966	5.520
91.4746001	57.9	6.084	10.50	404	26.93	6.665	49.6	2.817	5.685
91.4998489	60.0	6.286	10.48	381	27.22	7.146	51.3	2.929	5.705
91.5284947	64.4	5.978	9.282	410	27.43	6.683	50.0	2.902	5.809
91.5499415	57.5	5.632	9.789	407	27.06	6.652	51.0	2.904	5.692
91.5701730	69.1	6.534	9.450	429	26.85	6.255	55.0	2.995	5.444
91.5900283	70.6	6.198	8.779	439	26.88	6.118	54.6	2.945	5.392
91.6116892	69.6	6.429	9.234	431	27.18	6.300	56.0	3.020	5.391
91.6337262	61.5	5.822	9.463	430	26.88	6.254	53.5	2.846	5.319
91.6552135	62.0	5.940	9.580	425	26.95	6.340	54.5	3.078	5.651
91.6762725	70.4	5.612	7.977	449	25.98	5.780	56.1	2.827	5.041
91.6969612	82.6	6.332	7.667	456	26.55	5.821	59.9	3.030	5.223
91.7175572	78.2	6.221	7.959	466	26.04	5.583	56.6	2.827	4.997
91.7370827	72.0	6.132	8.514	418	27.33	6.535	50.7	2.890	5.701
91.7581764	59.9	6.266	10.46	399	28.19	7.061	50.5	3.007	5.949
92.4262725	67.7	5.688	8.400	411	26.05	6.345	52.2	2.707	5.185
92.4516776	63.5	6.100	9.610	428	27.80	6.494	54.9	2.833	5.160
92.4724531	63.2	6.223	9.844	446	28.63	6.413	56.7	2.905	5.120
92.4934542	66.9	6.119	9.142	447	29.16	6.521	54.2	2.873	5.304
92.5164461	68.2	6.082	8.921	453	29.54	6.522	55.1	2.878	5.226
92.5381012	74.5	6.409	8.602	470	29.49	6.270	58.0	3.007	5.181
92.5592702	79.1	5.986	7.563	470	27.75	5.901	58.2	2.797	4.808
92.5813998	82.3	6.382	7.751	520	27.68	5.318	65.5	2.824	4.311
92.6016660	94.5	6.392	6.762	524	27.22	5.198	66.3	2.729	4.115
92.6222563	93.0	6.451	6.933	510	28.06	5.499	65.1	2.842	4.365
92.6441545	89.3	6.687	7.485	505	27.66	5.479	64.6	2.933	4.537
92.6650746	89.8	5.994	6.672	518	25.71	4.959	66.6	2.701	4.058
92.6870017	85.8	6.848	7.983	476	28.52	5.987	56.2	2.721	4.841
92.7079970	80.8	5.447	6.742	503	25.41	5.054	57.5	2.464	4.287
92.7324183	76.7	5.171	6.740	487	24.54	5.044	66.3	2.643	3.987
92.7531591				490	26.29	5.364	61.2	2.710	4.425

[1]Line fluxes in units of 10^{-14} erg s^{-1} cm^{-2}.
[2]Continuum fluxes in units of 10^{-16} erg s^{-1} cm^{-2} Å^{-1}.

Poor centring either of the slit on the galaxy or of the extraction aperture during the data reduction could lead to variations in flux density. The use of two slits was intended primarily to take the former point into account: if the observed variability in the 2-arcsec slit data was solely a result of mis-centring of the galaxy in the slit, we would not expect this to be as significant a problem in the wider 8-arcsec slit data. Because the variability has similar shape and amplitude for both slits, we feel that we can confidently rule this out as the source of variability. Also, as mentioned above, the extraction aperture used during the data reduction was checked and no evidence that the aperture failed to collect all the light from the Seyfert nucleus or that the host galaxy contribution varied significantly was found.

Next, we checked whether any variations could be result from changes in seeing conditions during the observations. Three possibilities are considered here: (i) the variations are entirely the result of seeing changes; (ii) the source has some small intrinsic variability,

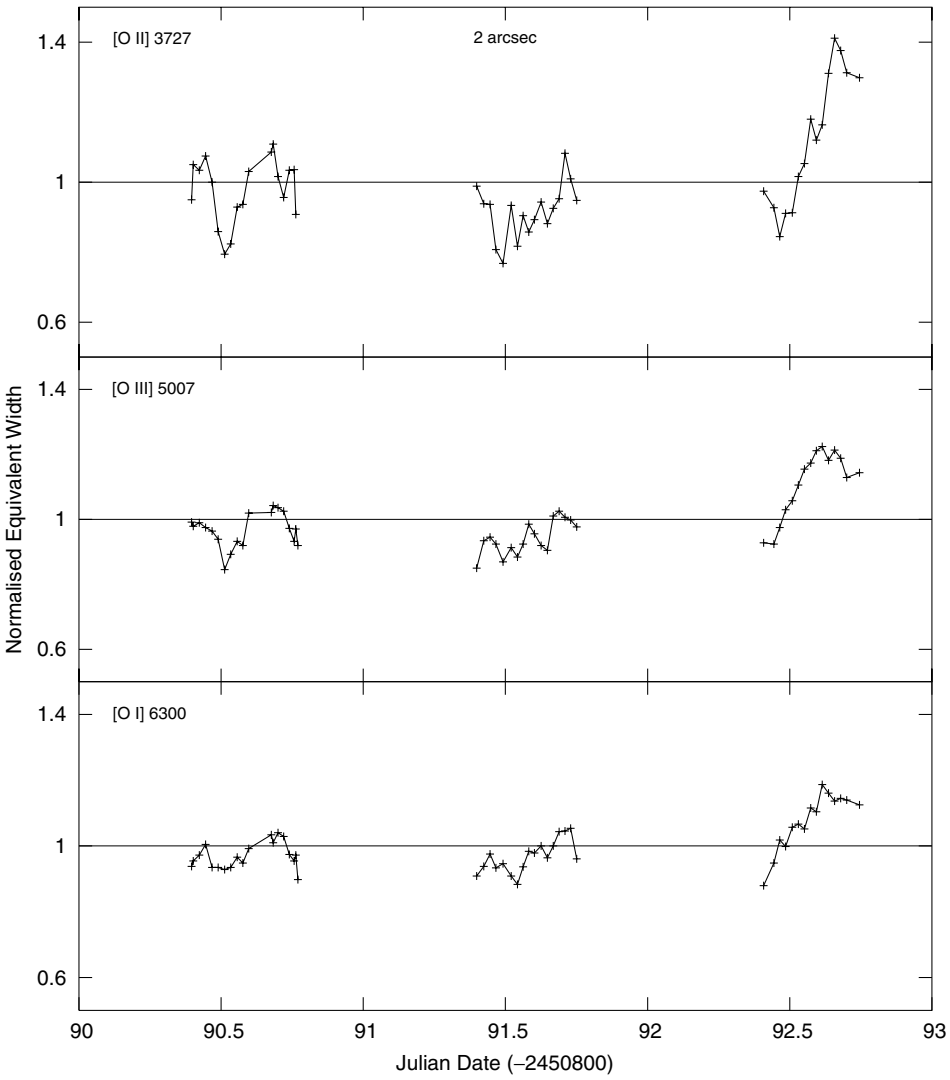

Figure 3. Equivalent widths (scaled using mean equivalent width) versus JD for the [O II] 3727-Å (top panel), [O III] 5007-Å (middle) and [O I] 6300-Å (bottom) lines measured using the 2-arcsec slit spectra.

but this is exaggerated by changes in flux brought about by changes in seeing; and (iii) the relative sizes of the NLR and continuum-emitting regions change depending on the seeing conditions. The first possibility can again be discounted by looking at the variations seen in both the 2- and 8-arcsec slit data. If the variability is entirely the result of seeing changes, one would expect that any variations seen in the 2-arcsec slit data would get washed out and be of considerably lower amplitude in the 8-arcsec slit data because even with poor seeing all of the nuclear light should pass through the wider slit. Also, because the equivalent width is a measure of the ratio between line and continuum flux, if all the variations in the line and continuum fluxes are entirely artificial and from the same source, we would expect to see no changes in the equivalent widths. In fact, the amplitude of variability in both data sets is similar and so changes in equivalent width cannot be entirely the result of changes in seeing.

It should be possible to determine whether any intrinsic source variations are exacerbated by variations as a result of poor seeing by investigating whether there is a correlation between the size of the seeing disc and the equivalent width measurement, because it might reasonably be expected that the magnitude of any effect would be directly related to the quality of the seeing at the time. To measure the size of the seeing disc directly, a narrow section of each NGC 4395 spectrum close to the [O III] 5007-Å emission line was extracted along the dispersion axis and a single Gaussian fit to the resulting cross-dispersive profile. The FWHM of this fit was then used as a direct measurement of the seeing throughout each night. The equivalent width measurements for the [O III] 5007-Å line are shown plotted versus FWHM in Fig. 7. No correlation between the parameters is seen. Because any effect should be most readily observed in the 2-arcsec slit data (shown here), we discount this as the source of the NGC 4395 variability.

In addition to the [O III] 5007-Å line, continuum sections close to the [O II] 3727- and [O I] 6300-Å lines were extracted and similar Gaussian fits applied to the cross-dispersive profiles. The same procedure was also applied to the spectral regions containing the lines themselves. Because the AGN core will be a blue point source whereas any host galaxy contamination will be from diffuse and relatively red starlight, comparing the FWHM of the blue and red continuum regions checks whether changes in the quality of the seeing affect the seeing disc for emission arising from different parts

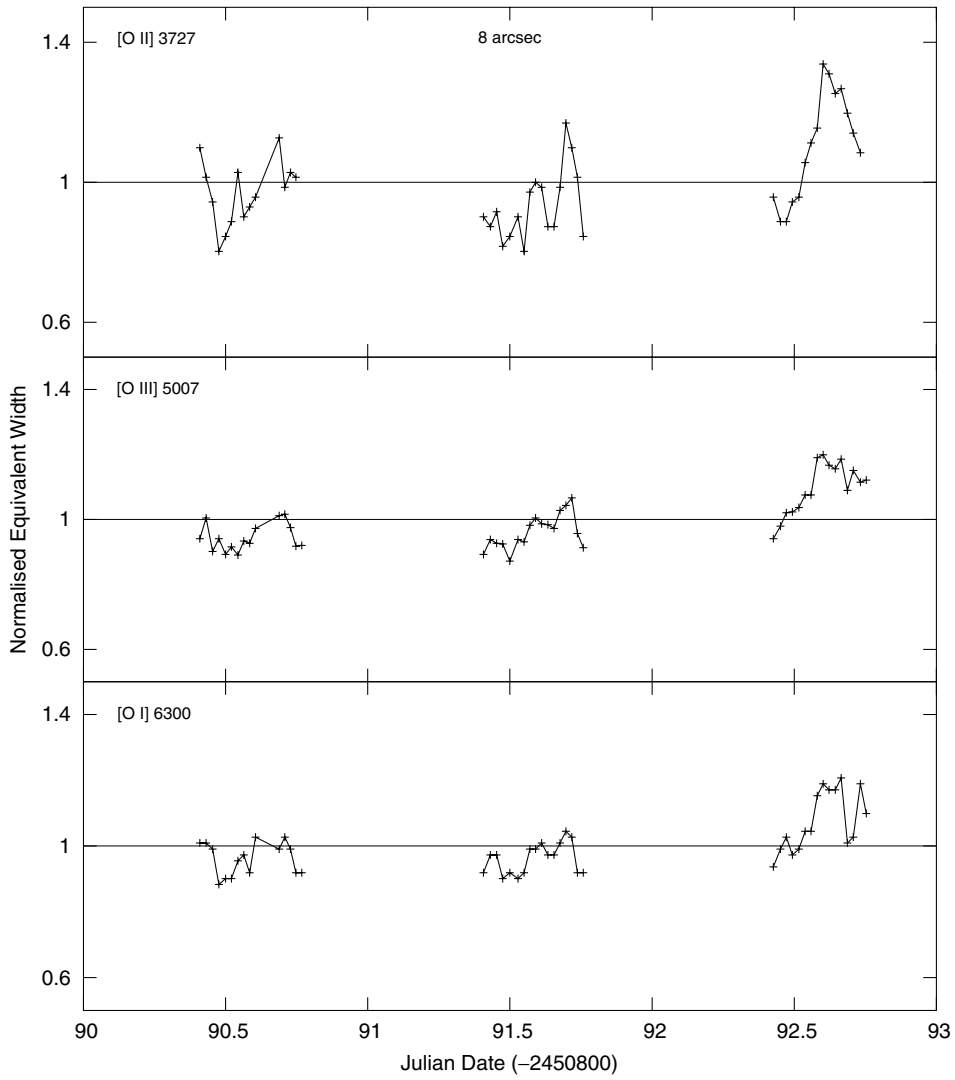

Figure 4. Equivalent widths (scaled using mean equivalent width) versus JD for the [O II] 3727-Å (top panel), [O III] 5007-Å (middle) and [O I] 6300-Å (bottom) lines measured using from the 8-arcsec slit spectra.

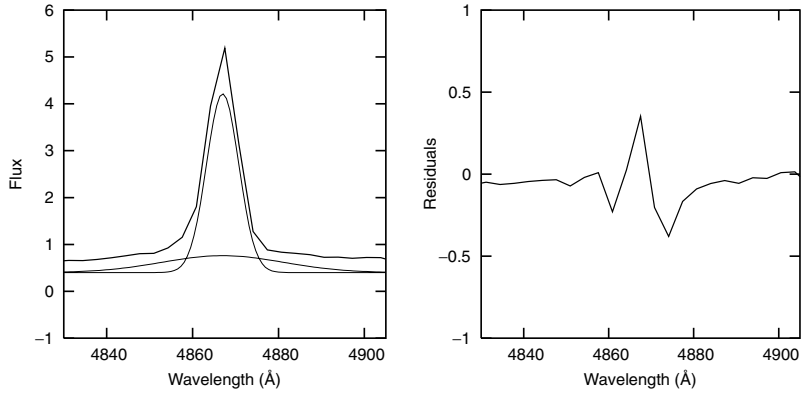

Figure 5. Example Gaussian fit to Hβ. The width of the narrow component had a fixed instrumental width measured from other lines, while the width of the broad component varied as a free parameter. All fluxes are in units of 10^{-15} erg cm^{-2} s^{-1} Å^{-1}.

of the nuclear region in different ways. The FWHM for the red and blue continuum regions are shown plotted against one another in Fig. 8, together with the 1:1 line for comparison. Similarly, changes in seeing could affect emission from the continuum-emitting source differently to emission from the NLR, which could be partially resolved under good conditions (although as mentioned in Section 2 this is unlikely). To test this, the FWHM for the extracted regions containing the [O III] 5007-Å emission line and nearby continuum

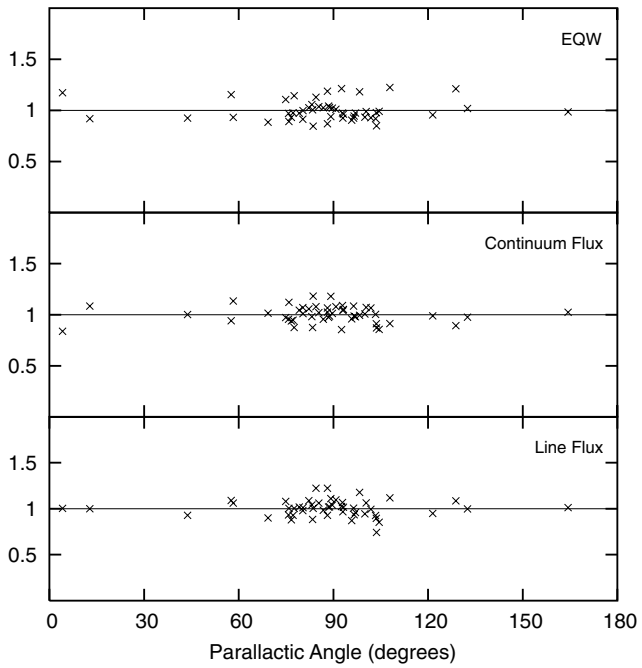

Figure 6. Normalized equivalent width (top panel), continuum flux (middle panel) and line flux (bottom panel) versus parallactic angle for the [O III] 5007 line as measured from the 2-arcsec slit data.

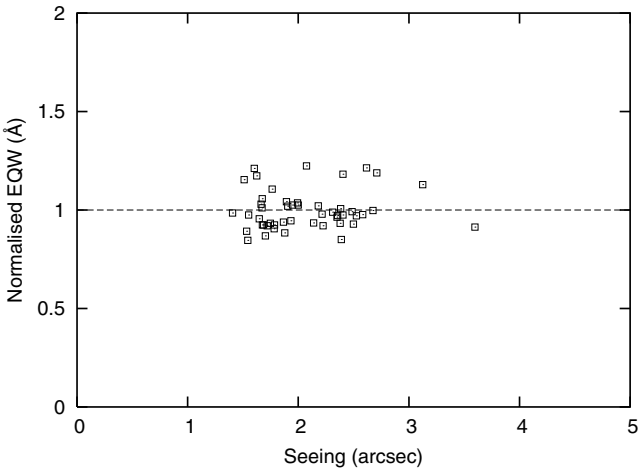

Figure 7. Normalized equivalent width versus the FWHM of the seeing disc. The EQW and FWHM measurements were made using the [O III] 5007 line from spectra taken using the 2-arcsec slit width.

region are shown plotted in Fig. 9, again with the 1:1 comparison line. There is no evidence in either Figs 8 or 9 for significant deviations from the 1:1 correlation, so from this we conclude that the seeing changes have not had a significant differential effect on emission from different regions and hence this is unlikely to be the source of the variability. From Fig. 9, we also conclude that the NLR is not resolved in any of the observations and so this is not likely to cause spurious variability.

The last remaining likely systematic error is atmospheric transparency variations. As discussed in Section 3.1, although we used standard star observations to correct trends, short time-scale variations could remain at the level of a few per cent. In the next section, we show that the scatter in measured line fluxes is consistent with

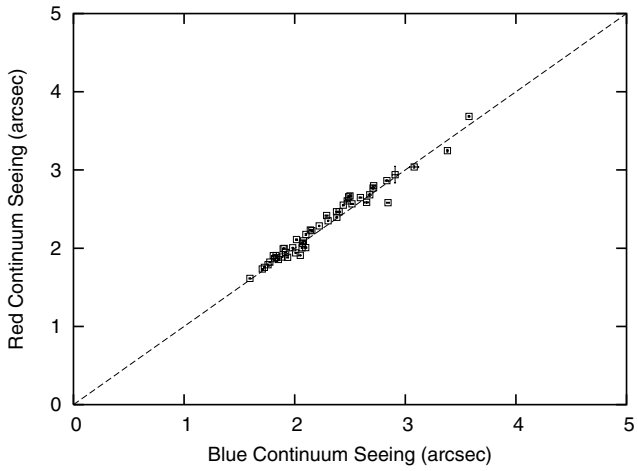

Figure 8. FWHM of the cross-dispersive profiles measured for the red continuum region against that of the blue continuum region, from the 2-arcsec slit spectra. Also shown is the 1:1 line for comparison.

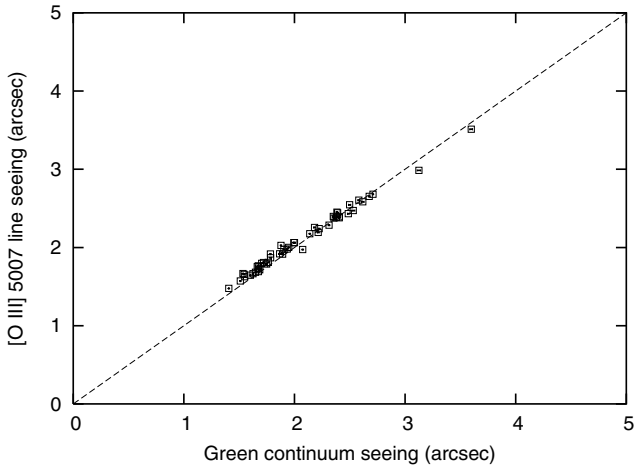

Figure 9. FWHM of the cross-dispersive profiles measured for the [O III] 5007 line and nearby continuum region. Again the 1:1 line is shown for comparison.

this effect, whereas continuum fluxes show a larger scatter. Overall then, we have considerable confidence that the continuum variations show real intrinsic variability of the nuclear source.

4.3 Variability analysis

Fig. 10 shows the mean-normalized line and continuum fluxes for the [O III] 5007-Å line measured from the 8-arcsec slit data. The absolute flux calibration accuracy achieved for the wider slit is ∼4 per cent for all three nights, based on the deviation of the [O III] 5007-Å line fluxes from the absolute flux calibration. The accuracy for the 2-arcsec slit data is somewhat lower because these data suffered from additional fluctuations attributed to changes in seeing across each night. The mean absolute line and continuum fluxes and fractional variation (defined as the ratio of the standard deviation and the mean flux) for the three narrow lines for which the equivalent widths were determined are given in Table 4. The figures for the 8-arcsec data clearly show larger variances in the continuum fluxes than in the line fluxes, suggesting intrinsic source variability. Fig. 11 shows the continuum and line fluxes plotted against one another. This not

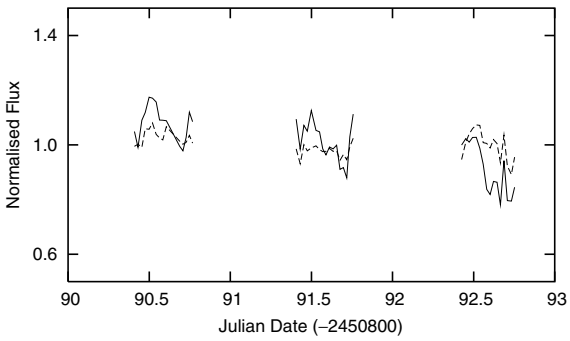

Figure 10. Mean-normalized [O III] 5007 line flux (dashed line) and continuum flux (solid line) for the 8-arcsec slit.

only shows the greater continuum variability, but also shows a correlation between the absolute flux measurements that suggests some small uncorrected systematic errors remain. This suggests the EQW will give the most accurate determination of intrinsic variability.

The optical light curves constructed using the EQW measurements in Tables 2 and 3 are shown in Figs 3 and 4 respectively, while the fractional variation in EQW for the three narrow lines and both slits are given in Table 5. The average sampling interval was 31.6 and 33.0 min for the 2- and 8-arcsec slit data respectively, and the large gaps in the light curve represent daylight periods. The light curves show that the nucleus in NGC 4395 varied significantly during the observing campaign, including over short (<8 h) time-scales, with the changes similar in shape for all three lines and for both slit widths. The largest variability occurs on night 3, with an ∼50 per cent increase in equivalent width (at [O II] 3727-Å) occurring over a time-scale of 5 h, corresponding to a decrease in continuum luminosity of 35 per cent. Similar variability, but with smaller amplitude, is also seen in the green and red continuum regions. Small amplitude (∼ few per cent) variability is seen over time-scales as short as the sampling interval, but given the measurement errors this is likely to be of only marginal significance.

To test whether there was any difference in the variability with colour, the EQW measurements for the [O II] 3727- and [O I] 6300-Å line were plotted against each other, as shown in Fig. 12. A least-squares fit was then performed in the usual way to determine the best-fitting straight line. The best-fitting solutions have gradients of 1.54 and 1.33 for the 2- and 8-arcsec data respectively, although a 1:1 relation gave a poorer fit (reduced $\chi^2 = 5.92$ for the 2-arcsec slit data) but could not entirely be ruled out. This suggests that there was greater variability in the [O II] 3727-Å EQW than the [O I] 6300-Å EQW, which is consistent with the findings of Clavel et al. (1991) that the spectra of AGN harden as they brighten. The effect could potentially be caused by starlight contamination, however the surface brightness of the host galaxy bulge is low, arguing against a large degree of contamination. The difference between the two lines is larger for the 2-arcsec data than the 8-arcsec data, which is consistent with the 8-arcsec data being affected more by contamination from the host galaxy starlight, suggesting a small but real residual colour effect.

No significant variability in the broad Hβ flux was observed. If the variability in NGC 4395 is qualitatively the same as that in other Seyfert 1 galaxies such as NGC 5548 (see Section 5), we would expect to see roughly the same variations in the Hβ line as the nearby continuum, with a lag induced by the light traveltime between the accretion disc and broad-line region (Peterson et al. 1992). However, the signal-to-noise ratio of the broad component is poor and proved difficult to fit a Gaussian profile to, so it is difficult to make quantitative statements. Fig. 13 shows the mean-normalized continuum flux measured for the [O III] 5007-Å line plotted against that for the Hβ broad component. The scatter is greater than that seen in Fig. 11, but there is still greater variance in the continuum flux than the broad Hβ flux. Fig. 14 shows the mean-normalized broad Hβ flux against the mean-normalized flux for the narrow component. The scatter is considerable for both parameters: the fractional variation over all three nights for the broad and narrow components is 5.9 and 9.5 per cent, respectively. The apparent correlation is expected and is a result of allowing the amplitude of both fitted Gaussians to vary as free parameters.

5 DISCUSSION

5.1 Comparison with NGC 5548

The short time-scale optical variability seen in NGC 4395 (shown in Figs 3 and 4) is extremely rare in Seyfert galaxies. This suggests that NGC 4395 does indeed have a small black hole rather than an extremely low accretion rate. Simultaneous X-ray and optical observations of another low-luminosity Seyfert 1, NGC 4051 (Done

Table 4. Line and continuum variability parameters.

Band	Night	2-arcsec slit				8-arcsec slit			
Å		$\bar{F}_l$ [a]	$\bar{F}_c$ [b]	$\sigma_l/\bar{F}_l$	$\sigma_c/\bar{F}_c$	$\bar{F}_l$ [a]	$\bar{F}_c$ [b]	$\sigma_l/\bar{F}_l$	$\sigma_c/\bar{F}_c$
[O II] 3727	1	5.429	9.040	0.073	0.096	6.515	9.500	0.061	0.088
	2	4.091	8.687	0.086	0.087	6.106	9.285	0.049	0.093
	3	5.611	8.228	0.136	0.104	6.132	7.943	0.067	0.133
	All	5.297	8.667	0.114	0.103	6.239	8.913	0.067	0.129
[O III] 5007	1	26.54	5.820	0.074	0.085	28.26	6.866	0.027	0.056
	2	25.13	5.638	0.077	0.058	26.93	6.423	0.022	0.068
	3	28.79	5.516	0.070	0.085	27.47	5.782	0.053	0.100
	All	26.72	5.670	0.091	0.080	27.53	6.348	0.041	0.102
[O I] 6300	1	2.812	4.721	0.093	0.097	3.125	5.861	0.033	0.058
	2	2.692	4.521	0.070	0.052	2.926	5.497	0.028	0.050
	3	2.977	4.519	0.078	0.089	2.785	4.686	0.046	0.096
	All	2.820	4.595	0.091	0.085	2.941	5.341	0.059	0.113

[a]Line fluxes in units of 10^{-14} erg s^{-1} cm^{-2}.
[b]Continuum fluxes in units of 10^{-16} erg s^{-1} cm^{-2} Å^{-1}.

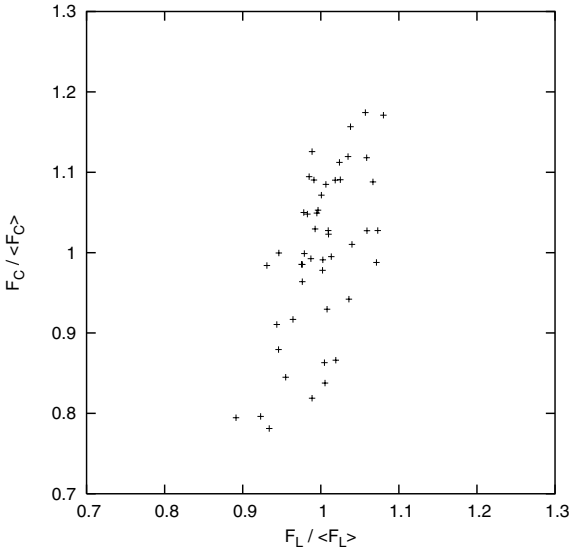

Figure 11. Normalized continuum flux versus normalized narrow line flux for the [O III] 5007 line measured from the 8-arcsec slit data.

Table 5. Fractional variation in the EQW measurements for the three narrow lines.

Band Å	Night	2-arcsec slit $\sigma_{EQW}/E\bar{Q}W$	8-arcsec slit $\sigma_{EQW}/E\bar{Q}W$
[O II] 3727	1	0.090	0.091
	2	0.081	0.104
	3	0.162	0.133
	All	0.147	0.135
[O III] 5007	1	0.053	0.043
	2	0.053	0.054
	3	0.090	0.070
	All	0.099	0.089
[O I] 6300	1	0.040	0.050
	2	0.050	0.047
	3	0.077	0.081
	All	0.075	0.083

et al. 1990), found no evidence for significant optical variability during a 6-d period in which the X-ray flux varied by up to a factor of 2. The total variability in the *B* band over the entire observing period was just 1.4 per cent, with the optical flux remaining constant to within 1 per cent during the periods of highest X-ray variability.

The variability of both continuum and emission lines in the Seyfert 1 galaxy NGC 5548 has been well studied at both ultraviolet (UV) and optical wavelengths in order to determine the structure of the unresolved emission line regions. NGC 5548 was monitored in the UV every 4 d for a total of 8 month using *International Ultraviolet Explorer* (*IUE*; Clavel et al. 1991) and every few days over a period of 10 month using a number of telescopes in the optical (Peterson et al. 1991). The large quantity of variability data at these wavelengths makes it an ideal object to use as a comparison with NGC 4395.

To compare NGC 4395 and 5548, the variability PDS for NGC 5548 for the UV light curve was obtained from Krolik et al. (1991). The stochastic nature of the variability in AGN means that the PDS is the best way to probe the distribution of variability amplitude with time-scale. Given that the effect of red noise means that the

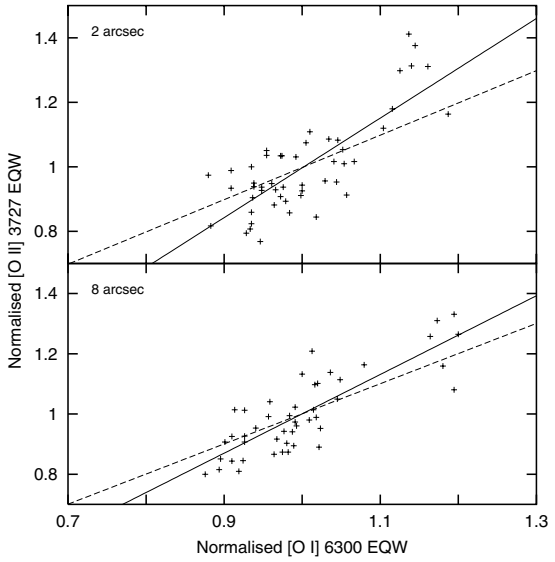

Figure 12. [O II] 3727 normalized equivalent width versus [O I] 6300 normalized equivalent width for both the 2-arcsec slit (top) and 8-arcsec slit (bottom). In both cases, the solid line represents the best-fitting straight line through the points and the dashed line represents the 1:1 gradient correlation. The gradients of the best-fitting lines are 1.54 and 1.33 for the 2- and 8-arcsec slit data, respectively.

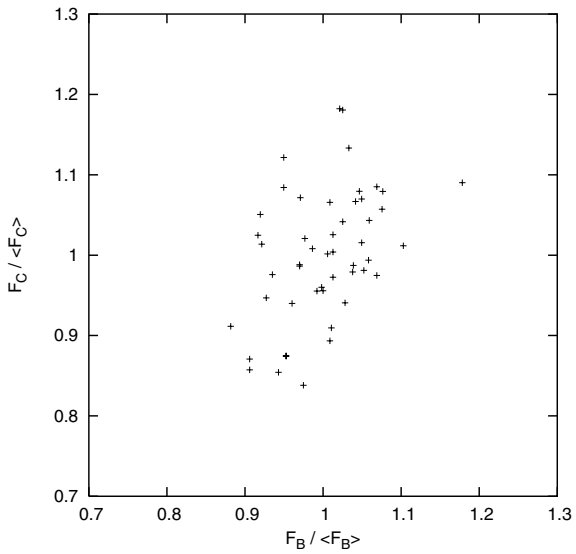

Figure 13. Normalized continuum flux measured under the [O III] 5007 line (using a low-order polynomial fit to the continuum) versus the normalized flux measured for the broad component of the Hβ line. Measured using the 2-arcsec slit data.

variability amplitude depends on the observation length, the PDS slope must be known before the fractional variability of two objects can be compared. Here, we assume that the slopes of the PDS for NGC 5548 and 4395 are the same and that the difference in black hole mass changes the frequency scaling, resulting in a change in the PDS normalization at a given frequency. This is consistent with the recent results of Vaughan et al. (2004), who suggest that the large X-ray variability amplitudes seen in both NGC 4051 and 4395 could be the result of the power spectra in these objects being shifted to higher frequencies in comparison with AGN with more massive black holes.

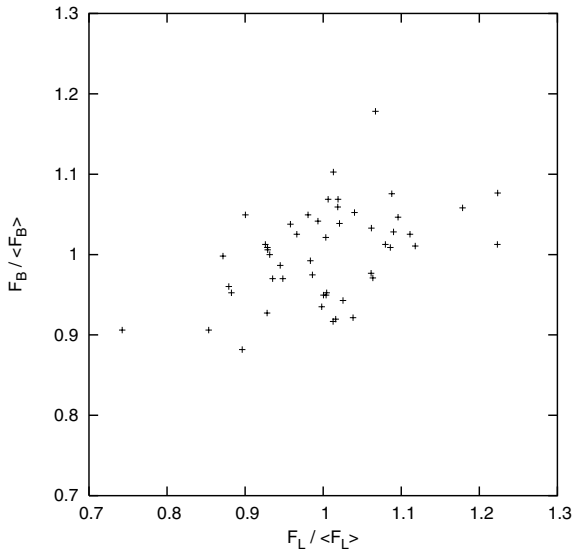

Figure 14. Normalized flux for the broad component of the Hβ line versus line flux measured for the [O III] 5007 line. Measured using the 2-arcsec slit data.

A power law of the form $P(\nu) = K\nu^{-\alpha}$ was fitted to the NGC 5548 PDS. The final few points are noisy as a result of the 4-d sampling interval and so these were excluded from the fit. The best-fitting solution gave a power-law index of $\alpha = 2.8$, which was used to extend the PDS to the higher frequencies sampled by the NGC 4395 light curves discussed here. Because the UV fluctuations for NGC 5548 have larger amplitude than the optical fluctuations, the normalization of the UV PDS was scaled using the ratio between the fractional variations for the UV and optical light curves calculated using the data from Clavel et al. (1991) and Peterson et al. (1991), respectively. To avoid the effects of red noise on the variances, data sets of the same length were used for this.

The scaled PDS was used to calculate the expected variances in the optical light curves for NGC 5548 over time-scales of 8 and 72 h. The expected fractional variations over these time-scales were calculated to be 0.04 and 0.3 per cent, respectively. The process was repeated, this time using the original UV PDS, and the expected fractional variations in the UV for NGC 5548 were calculated to be 0.09 per cent (8 h) and 0.7 per cent (72 h). Neither the expected optical or UV fractional variability for NGC 5548 is consistent with the 6–13 per cent variation observed in the continuum flux for NGC 4395. This analysis confirms that NGC 4395 has larger short time-scale variability than other Seyfert galaxies. A similar result holds in X-rays (Iwasawa et al. 2000; Shih et al. 2003). It seems plausible that this is because the black hole is smaller and so time-scales are shorter. In the next section, we address this question quantitatively.

5.2 Does variability scale with black hole mass?

The precise relationship between variability and black hole mass is dependent upon the precise origin of the variability. If the time-scales for variability are dictated principally by the light traveltime across the accretion disc, then one might expect a direct scaling between variability time-scale and black hole mass. Considering a more detailed model in which the time-scale for variability at different wavelengths is dictated by the sound-crossing time-scale gives a different answer; this is discussed below.

To investigate direct scaling between black hole mass and variability, we assume that the slope of the variability power spectra for both NGC 4395 and 5548 are the same, and that the different black hole masses result in a simple translation of the power spectrum along the frequency axis. Then the ratio of black hole mass can be used to predict the variability that we would see in NGC 4395 using the NGC 5548 variability for which the power spectrum is already known. We use black hole masses of $10^5\,\mathrm{M}_\odot$ (Kraemer et al. 1999; Shih et al. 2003) and $6.1 \times 10^7\,\mathrm{M}_\odot$ (Wandel, Peterson & Malkan 1999) for NGC 4395 and 5548, respectively. This implies that a time-scale of 200 d in NGC 5548 should correspond to a time-scale of 8 h in NGC 4395. Using the UV power spectrum for NGC 5548 we find that variability of 29 per cent is expected over this time-scale. This is much larger than the variability seen for NGC 4395 over an 8-h period for any optical wavelength. If however we consider the optical variability of NGC 5548 over 200 d, we expect variability of order 12 per cent, which is much closer to that seen in NGC 4395. It is unclear at present whether a direct scaling of the two power spectra is valid. Consequently, we have also investigated a more detailed model in which we have attempted to take some of the properties of the accretion disc into account.

We have modelled the central engine of NGC 4395 using a simple accretion disc for which the emitted spectrum is a sum of blackbodies. Considering the release of thermal binding energy at a radius R gives a blackbody effective temperature of

$$T(R) = \left(\frac{GM_{\mathrm{BH}}\dot{m}}{8\pi R^3\sigma}\right)^4, \tag{1}$$

where M_{BH} is the mass of the central black hole, $\dot{m}$ is the accretion rate, σ is the Stefan–Boltzmann constant and all other symbols take their usual values. Obviously the precise formula for $T(R)$ depends on the specific model adopted, but the binding energy formula should be good enough for our approximate scaling calculation below. If we assume that the nucleus is time steady and has an accretion rate $\dot{m} = (6.32M_{\mathrm{BH}}/\eta c^2)(L/L_{\mathrm{E}})$ (in SI units), where L_{E} is the Eddington luminosity, the above temperature relation then gives

$$R^3 \propto \frac{M_{\mathrm{BH}}^2}{T^4}\left(\frac{L}{L_{\mathrm{E}}}\right). \tag{2}$$

If the size of the emitting region and the variability time-scale scales with black hole mass, then it should be possible to calculate the scaling factor for NGC 4395 and 5548. We use an accretion rate of $0.0017L_E$ (Lira et al. 1999) for NGC 4395 and an accretion rate of $0.015L_E$ for NGC 5548 (Wandel et al. 1999). From equation (2), we find that for a fixed wavelength (and hence temperature) the time-scales for variability for the two objects should scale by a factor $(6.1 \times 10^7/10^5)^{2/3}(0.015/0.0017)^{1/3} = 149$. So a time-scale of 8 h in NGC 4395 (i.e. one observing night) should correspond to approximately 50 nights for NGC 5548. A randomly selected sample of 10 sections of 50 d from the optical flux values given in table 9 of Peterson et al. (1991) gives an average fractional deviation of 10.9 per cent. This value agrees well with the average fractional deviation of 10.0 per cent in the [O II] 3727-Å EQW measurements for NGC 4395 over time-scales of one night. This shows that the anomalous variability of NGC 4395 is quantitatively consistent with that expected for a small central black hole.

5.3 Absolute variability time-scales

Above we showed that the relative variability of NGC 4395 is consistent with simple accretion disc models. However, there are problems

when we consider the absolute variability time-scales. Considering the light- and sound-crossing time-scales for a particular black hole mass gives lower and upper limits on the time-scales for variability using $R \propto M_{\rm BH}^{2/3} \propto \Delta t$. If the mass of the central engine in NGC 4395 is of the order $10^5\,{\rm M}_\odot$ and the temperature of order 10^4 K, then using a value of 10^4 ms^{-1} for the sound speed gives a light-crossing time-scale of 28 min and sound-crossing time-scale of 1.6 yr for the time-steady, Eddington-limited case if the optical emission is emitted at $1720R_S$. A more realistic estimate (Lira et al. 1999) puts the accretion rate at $\sim 10^{-3} L^{\rm E}$, giving light- and sound-crossing time-scales of 2.8 min and 59 d, respectively. Instabilities in the disc would be expected to propagate at the sound speed and therefore we would not expect to see variability on time-scales shorter than this. This shows that variability time-scale is therefore a problem for NGC 4395 as it is for other Seyfert galaxies.

6 SUMMARY AND CONCLUSIONS

We present optical spectroscopic data for the least-luminous Seyfert 1, NGC 4395, covering three nights during which the nucleus was observed approximately every 30 min. Two slit widths were used, enabling us to minimize or quantify systematic errors and aperture effects, giving an absolute flux calibration accuracy of 5–10 per cent. To reduce the effect of any remaining systematic errors, equivalent width measurements of three narrow lines in the blue, green and red regions of the spectrum were used to quantify the continuum variability, while absolute measurements of the broad-component flux of the Hβ line were used to constrain variability in the broad lines.

The continuum in NGC 4395 was variable over all three nights, with the greatest amplitude of variability occurring during night 3. The variability appeared to be simultaneous for all three continuum regions, with greater variability seen in the continuum flux under the [O II] 3727-Å line than the continuum under the [O I] 6300-Å line. The observed hardening of the spectrum with increasing luminosity is consistent with the findings of Clavel et al. (1991), although contamination by starlight cannot be completely ruled out. No measurable variability was detected in the broad Hβ flux.

The nucleus in NGC 4395 was compared with another well-studied Seyfert 1, NGC 5548. NGC 4395 was found to vary with greater amplitude over shorter time-scales than NGC 5548. A simple accretion disc model was used to calculate the expected scaling between NGC 4395 and 5548 if the time-scale for variability scaled with the mass of the central black hole, and the results were consistent with the observed optical variability for NGC 5548 if NGC 4395 has a black hole with a mass approximately 2 orders of magnitude smaller than that for NGC 5548. The observed variability was not consistent with the expected absolute time-scales for variability if instabilities propagate through the accretion disc at sound speed.

ACKNOWLEDGMENTS

JES acknowledges a PPARC research studentship. The Isaac Newton Telescope is operated on the island of La Palma by the Royal Greenwich Observatory in the Spanish Observatorio del Roque de los Muchachos of the Instituto de Astrofisica de Canarias. IRAF is distributed by the National Optical Astronomy Observatories, which are operated by AURA, Inc., under cooperative agreement with the National Science Foundation.

REFERENCES

Almaini O. et al., 2000, MNRAS, 315, 325
Clavel J. et al., 1991, ApJ, 366, 64
Done C., Ward J. M., Fabian A. C., Kunieda H., Tsuruta S., Lawrence A., Smith M. G., Wamsteker W., 1990, MNRAS, 243, 713
Ferrarese L., Merritt D., 2000, ApJ, 539, L9
Filippenko A. V., Ho L. C., 2003, ApJ, 588, L13
Filippenko A. V., Sargent W. L. W., 1989, ApJ, 342, L11
Filippenko A. V., Ho L. C., Sargent W. L., 1993, ApJ, 410, L75
Gebhardt K. et al., 2000, ApJ, 539, L13
Iwasawa K., Fabian A. C., Almaini O., Lira P., Lawrence A., Hayashida K., Inoue H., 2000, MNRAS, 318, 879
Kraemer S. B., Ho L. C., Crenshaw D. M., Shields J. C., Filippenko A. V., 1999, ApJ, 520, 564
Krolik J. H., Horne K., Kallman T. R., Malkan M. A., Edelson R. A., Kriss G. A., 1991, ApJ, 371, 541
Lira P., Lawrence A., O'Brien P., Johnson R. A., Terlevich R., Bannister N., 1999, MNRAS, 305, 109
Manners J. C., Almaini O., Lawrence A., 2002, MNRAS, 330, 390
Massey P., Strobel K., Barnes J. V., Anderson E., 1988, ApJ, 328, 315
Moran E. C., Filippenko A. V., Ho L. C., Shields J. C., Belloni T., Comastri A., Snowden S. L., Sramek R. A., 1999, PASP, 111, 801
Nandra K., George I. M., Mushotzky R. F., Turner T. J., Yaqoob T., 1997, ApJ, 476, 70
Oke J. B., 1990, AJ, 99, 1621
Peterson B. M. et al., 1991, ApJ, 368, 119
Peterson B. M. et al., 1992, ApJ, 392, 470
Peterson B. M. et al., 2000, ApJ, 542, 161
Ptak A., Yaqoob T., Mushotzky R., Serlemitsos P., Griffiths R., 1998, ApJ, 501, L37
Shields J. C., Filippenko A. V., 1992, in Filippenko A. V., ed., ASP Conf. Ser. Vol. 31, Relationships between Active Galactic Nuclei and Starburst Galaxies. Astron. Soc. Pac., San Francisco, p. 267
Shih D. C., Iwasawa K., Fabian A. C., 2003, MNRAS, 341, 973
Sramek R., 1992 in Filippenko A. V., ed., ASP Conf. Ser. Vol. 31, Relationships between Active Galactic Nuclei and Starburst Galaxies. Astron. Soc. Pac., San Francisco, p. 273
Turner T. J., George I. M., Nandra K., Turcan D., 1999, ApJ, 524, 667
Vaughan S., Iwasawa K., Fabian A. C., Hayashida K., 2004, MNRAS, 356, 524
Wandel A., Peterson B. M., Malkan M. A., 1999, ApJ, 526, 579

This paper has been typeset from a TEX/LATEX file prepared by the author.